

**Polyradical character and spin frustration in
fullerene molecules:
An *ab initio* non-collinear Hartree–Fock study**

Carlos A. Jiménez-Hoyos,^{*,†} R. Rodríguez-Guzmán,^{†,‡} and Gustavo E.
Scuseria^{†,‡}

*Department of Chemistry, Rice University, Houston, TX 77005, and Department of Physics and
Astronomy, Rice University, Houston, TX 77005*

E-mail: jimenez.hoyos@gmail.com

^{*}To whom correspondence should be addressed

[†]Department of Chemistry, Rice University, Houston, TX 77005

[‡]Department of Physics and Astronomy, Rice University, Houston, TX 77005

Abstract

Most *ab initio* calculations on fullerene molecules have been carried out based on the paradigm of the Hückel model. This is consistent with the restricted nature of the independent-particle model underlying such calculations, even in single-reference-based correlated approaches. On the other hand, previous works on some of these molecules using model Hamiltonians have clearly indicated the importance of short-range inter-atomic spin-spin correlations. In this work, we consider *ab initio* non-collinear Hartree–Fock (HF) solutions for representative fullerene systems: the bowl, cage, ring, and pentagon isomers of C_{20} , and the larger C_{30} , C_{36} , C_{60} , C_{70} , and C_{84} fullerene cages. In all cases but the ring we find that the HF minimum corresponds to a truly non-collinear solution with a torsional spin density wave. Optimized geometries at the generalized HF (GHF) level lead to fully symmetric structures, even in those cases where Jahn-Teller distortions have been previously considered. The nature of the GHF solutions is consistent with the π -electron space becoming polyradical in nature: each p -orbital remains effectively singly occupied. The spin frustration, induced by the pentagon rings in an otherwise anti-ferromagnetic background, is minimized at the HF level by aligning the spins in non-collinear arrangements. The long-range magnetic ordering observed is reminiscent of the character of broken symmetry HF solutions in polyacene systems.

1 Introduction

The discovery of fullerenes [1, 2] and their isolation in macroscopic quantities [3] has attracted interest in their electronic structure due to their unusual topology and curvature. C_{60} was expected to be the first example of a spherical aromatic molecule, but its properties turned out not to be consistent with this perspective. In particular, C_{60} and other fullerene compounds have chemical properties more similar to reactive alkene molecules than to aromatic systems [4].

Based on the inherent limitations conferred by the typical sizes of fullerene molecules, *ab initio* quantum chemical calculations on them are typically performed using a restricted formalism (see, *e.g.*, Refs. [5, 6]) either based on Hartree–Fock (HF) or density functional approxima-

tions. There has been little reason to question this strategy since some of the most common, stable fullerene molecules are non-magnetic and display a large HOMO-LUMO gap. On the other hand, it has sporadically been noted that some particular fullerene isomers (those with degeneracies in a Hückel-type approach) possess large multi-reference character. It was only recently reported by Stück *et al.* [7] that the restricted HF (RHF) solution for C_{60} is unstable, *i.e.*, there exists a broken-symmetry solution which is lower in energy. For the D_{6h} configuration of C_{36} , Varganov and co-workers [8] had similarly reported a triplet instability.

Stück *et al.* were seemingly unaware that the triplet instability of C_{60} was originally reported by Sheka [9] in semi-empirical calculations. In a series of works [9–13], Sheka and collaborators have interpreted the physical and chemical properties of fullerenes in terms of the unrestricted HF (UHF) solutions. She has advocated an *odd electron* (or polyradical) interpretation of the π -electron bonding in fullerenes, as opposed to the electron-gas picture obtained within a Hückel-type restricted formalism. She has also described C_{60} -based binary systems in terms of the donor–acceptor interactions between the corresponding species [14, 15]. Indeed, our interpretation of the bonding in fullerenes in this contribution follows the lines already elaborated by Sheka since 2004. The main difference lies in the use of non-collinear spins, which leads to a fully symmetric I_h configuration for C_{60} , consistent with a single ^{13}C -NMR peak [16], as opposed to the lesser symmetry present in UHF.

At this point we want to mention that the non-collinear arrangement of spins in C_{60} was originally described by Coffey and Trugman [17] in the framework of the classical Heisenberg Hamiltonian solution. Konstantinidis [18, 19] has more recently discussed the unconventional magnetic properties developed in spin lattices with icosahedral symmetry, such as that of C_{60} . Several papers [20–30] studied C_{60} using the Hubbard [31] and Pariser-Parr-Pople (PPP) [32, 33] model Hamiltonians following Coffey and Trugman’s original work. These emphasized the intermediate-to-strongly correlated nature of the physical system. We note that fully non-collinear HF solutions [20, 28] to the Hubbard Hamiltonian displayed, for sufficiently large U/t , the same type of spin arrangements observed in the classical Heisenberg description. It remained unclear, however,

whether a full-electron calculation would lead to the same type of mean-field solutions. In particular, Willaime and Falicov [23] observed that inclusion of Ohno-type screening lead to the normal paramagnetic state in PPP calculations with physical parameters.

The model Hamiltonian results stressed the role of anti-ferromagnetic spin-spin correlations in fullerene lattices. It is crucial to stress that a restricted-type solution is incompatible with the importance of spin-spin correlations. In particular, RHF overemphasizes bond alternation (or bond localization) and no spin ordering beyond that in the (localized) π -bond. Quantum Monte Carlo [22, 24, 26] results in a Hubbard framework have determined that spin-spin correlations in C_{60} are mid-ranged in nature (3-4 bonds), as opposed to the longer correlation length predicted by a mean-field broken symmetry treatment [20].

We shall also mention the work of a few quantum chemists in trying to understand the nature of the chemical bonding in fullerene molecules from a valence bond treatment of the Heisenberg Hamiltonian (see Ref. [34] and references therein). These studies have helped to rationalize the preference of π -electron density in C_{60} to lie on 6-6 bonds, which explains the observed reactivity patterns. They have also noted the importance of anti-ferromagnetic spin-spin correlations and how these can be well described in terms of the resonance of valence bond structures such as those characterizing the Kekulé basis.

In recent *ab initio* studies, the electronic structure of polyacene molecules composed of linearly fused benzene units has been investigated [35–41]. In particular, we and others have discussed how these systems become polyradical in nature using multi-reference *ab initio* methods. According to Hachmann *et al.* [35], the nature of the chemical bond in the π -space of polyacene molecules is best understood in terms of a localized resonating valence bond structure, rather than a more traditional delocalized-electron picture which would give rise to metallic-like behavior. We note that even HF predicts, in its own poor-man’s approach, the polyradical character of these systems: a RHF solution becomes unstable towards a UHF description in which electrons localize in the p orbitals of the carbon atoms according to an anti-ferromagnetic pattern. The broken symmetry HF description is characterized by long-range magnetic ordering.

In light of all these previous works, we decided to try a broken symmetry HF approach for the fullerene systems in full *ab initio* calculations. It was natural to consider non-collinear type solutions given the frustration induced by the presence of pentagon rings or, equivalently, the curvature present in these structures. Such an orientation can only be described in the framework of generalized HF (GHF) solutions [42–45], where each molecular orbital becomes a spinor. That is, each molecular orbital $\phi_i(\mathbf{r})$ is expanded, in the linear-combination of atomic orbitals (LCAO) approach, as

$$\phi_i(\mathbf{r}) = \sum_{\mu} (C_{\mu\uparrow,i} |\uparrow\rangle + C_{\mu\downarrow,i} |\downarrow\rangle) \chi_{\mu}(\mathbf{r}), \quad (1)$$

where $\chi_{\mu}(\mathbf{r})$ is an atom-centered basis function and $C_{\mu\uparrow,i}$ and $C_{\mu\downarrow,i}$ are independent coefficients. The use of GHF solutions in chemistry has been rather sparse. We recently noted [46] that GHF solutions must be invoked in order to fix the size-consistency problem of UHF in certain molecules, such as O₂. Yamaguchi and coworkers (see, *e.g.*, Refs. [47, 48]) have described how non-collinear HF solutions appear naturally in frustrated systems involving metal centers or organic radicals. Interestingly enough, in Ref. [47] GHF-type solutions were described for small carbon clusters. It was anticipated that a non-collinear solution would be suppressed in C₆₀ due to bond alternation, in spite of the presence of pentagon rings.

In this work we show, in full *ab initio* calculations, that HF affords broken symmetry solutions of the generalized type for fullerene molecules which are lower in energy than their RHF or UHF counterparts. We explore the nature of these solutions in terms of the arrangement of the localized spins in order to minimize the frustration induced by the presence of pentagon rings. We discuss how HF predicts these localized spins to interact via short-range spin-spin interactions, thus giving a picture consistent with previous model Hamiltonian results. These spin-spin interactions induce long-range magnetic ordering in the HF solution, leading to an overall polyradical character in the system. Lastly, we stress on the importance to carry out a spin projection in order to remove the unphysical effects associated with UHF or GHF solutions.

2 Computational details

We have performed RHF, UHF, and GHF geometry optimizations using a modified version of the `Gaussian 09` [49] suite of programs. The corresponding HF wave functions have been obtained using a quasi-Newton optimization method [50]. The 6-31G(*d*) and the 6-311G(*d*) basis sets, using Cartesian gaussian functions, were used in the calculations. Real orbitals were used with RHF and UHF, but complex solutions were used for GHF¹. We verified that the RHF and UHF solutions obtained were stable (in the Slater determinant space) and that the corresponding optimized geometries were true local minima. Unfortunately we were not able to perform such tests in GHF wave functions and geometries, as `Gaussian 09` currently lacks such capabilities.

For selected systems we have computed single-point symmetry-projected HF [51] energies and/or natural orbital occupations resulting from the optimized GHF solutions. We use the acronym S-GHF to denote *spin* (S) projected calculations out of GHF-type solutions. Here, the spin symmetry projection was carried out using the “transfer” operators

$$\hat{P}_{mk}^s = \frac{2s+1}{8\pi^2} \int d\Omega D_{mk}^{s*}(\Omega) \hat{R}(\Omega), \quad (2)$$

where $\Omega = (\alpha, \beta, \gamma)$ is the set of Euler angles, $D_{mk}^s(\Omega)$ are Wigner matrices, and

$$\hat{R}(\Omega) = \exp(-i\alpha\hat{S}_z) \exp(-i\beta\hat{S}_y) \exp(-i\gamma\hat{S}_z) \quad (3)$$

is the spin rotation operator. Note that the S-GHF wavefunction is written as a superposition of nonorthogonal Slater determinants. The projector above was discretized using sufficient points to converge expectation values such as $\langle \hat{S}^2 \rangle$ to high accuracy (10^{-8} or better). Due to their expensive nature, all the calculations in this work are in a projection-after-variation framework [51], using the GHF orbitals without further reoptimization. Such calculations were carried out using an in-house program [52].

¹Note that complex solutions are required in order to allow the spin orientations to adopt a 3D structure.

We have used the structures provided on Ref. [53] as initial guess geometries for some of the fullerenes considered. The Schlegel diagrams used in some of the figures were prepared with the help of the `Fullerene` program [54]. The molecular structure images shown in this paper, as well as the figure displayed in the table of contents, were prepared using `XCrySDen` [55].

Population analysis. Expectation values of one-body operators can be computed using the one-particle density matrix. For instance, the expectation values of the spin operators \hat{S}_x , \hat{S}_y , and \hat{S}_z are given by

$$\langle \hat{\mathbf{S}} \rangle = \frac{1}{2} \sum_{\mu\nu} \sum_{ss'} \sigma_{ss'} S_{\mu\nu} \gamma_{\nu s', \mu s}^1, \quad (4)$$

where S is the overlap matrix, σ are the Pauli matrices, and γ^1 is the one-particle density matrix in the atomic spin-orbital basis. The latter is related to the real-space one-particle reduced density matrix [56] by

$$\begin{aligned} \Gamma^1(\mathbf{r}s, \mathbf{r}'s') &\equiv N \int d\mathbf{x}_2 \cdots d\mathbf{x}_N \Psi^*(\mathbf{r}s, \mathbf{x}_2, \dots, \mathbf{x}_N) \Psi(\mathbf{r}'s', \mathbf{x}_2, \dots, \mathbf{x}_N) \\ &= \sum_{\mu\nu} \gamma_{\nu s', \mu s}^1 \chi_\mu^*(\mathbf{r}) \chi_\nu(\mathbf{r}'), \end{aligned} \quad (5)$$

where N is the number of electrons in the system.

We define an atomic magnetic moment \mathbf{M}_A using a Mulliken-like scheme, where $S_{\mu\nu} \gamma_{\nu s', \mu s}^1$ is interpreted as a population matrix [57, 58]. The magnetic moments are given by

$$\begin{aligned} \mathbf{M}_A &= \frac{1}{4} \sum_{\mu \in A, \nu} \sum_{ss'} \sigma_{ss'} S_{\mu\nu} \gamma_{\nu s', \mu s}^1 \\ &\quad + \frac{1}{4} \sum_{\nu \in A, \mu} \sum_{ss'} \sigma_{ss'} S_{\mu\nu} \gamma_{\nu s', \mu s}^1, \end{aligned} \quad (6)$$

where a symmetrization was done (compared to the standard Mulliken scheme) in order to obtain real values for \mathbf{M}_A . Note that, as long as only atom-centered functions are used, the sum of the atomic magnetic moments is equal to the corresponding spin expectation value, i.e., $\langle \hat{S}_z \rangle = \sum_A M_A^z$.

Expectation values of two-body operators can be computed, analogously, using the two-particle

density matrix. For instance,

$$\langle \hat{S}^2 \rangle = \frac{1}{2} \sum_{\mu \nu \lambda \kappa} \sum_{j=x,y,z} \sum_{s_1 s'_1} \sum_{s_2 s'_2} \sigma_{s_1 s'_1}^j \sigma_{s_2 s'_2}^j S_{\mu \nu} S_{\lambda \kappa} \tilde{\gamma}_{\nu s'_1 \kappa s'_2, \mu s_1 \lambda s_2}^2, \quad (7)$$

where

$$\gamma_{\nu s'_1 \kappa s'_2, \mu s_1 \lambda s_2}^2 = \tilde{\gamma}_{\nu s'_1 \kappa s'_2, \mu s_1 \lambda s_2}^2 - \frac{1}{2} \gamma_{\kappa s'_2, \mu s_1}^1 S_{\nu \lambda}^{-1} \delta_{s'_1 s_2} \quad (8)$$

is the two-particle density matrix in the atomic spin-orbital basis (normalized to the number of independent electron pairs). The latter is related to the real-space two-particle reduced density matrix [56] by

$$\Gamma^2(\mathbf{r}_1 s_1 \mathbf{r}_2 s_2, \mathbf{r}'_1 s'_1 \mathbf{r}'_2 s'_2) = \sum_{\mu \nu} \gamma_{\nu s'_1 \kappa s'_2, \mu s_1 \lambda s_2}^2 \chi_{\mu}^*(\mathbf{r}_1) \chi_{\lambda}^*(\mathbf{r}_2) \chi_{\nu}(\mathbf{r}'_1) \chi_{\kappa}(\mathbf{r}'_2). \quad (9)$$

Analogous to the one-particle case, one can interpret $S_{\mu \nu} S_{\lambda \kappa} \gamma_{\nu s'_1 \kappa s'_2, \mu s_1 \lambda s_2}^2$ as a two-electron population matrix. We compute atomic spin-spin correlations $\mathbf{S}_A \cdot \mathbf{S}_B$ in the form

$$\begin{aligned} \mathbf{S}_A \cdot \mathbf{S}_B = & \frac{1}{4} \sum_{\mu \in A, \lambda \in B} \sum_{\nu \kappa} \sum_{j=x,y,z} \sum_{s_1 s'_1} \sum_{s_2 s'_2} \sigma_{s_1 s'_1}^j \sigma_{s_2 s'_2}^j S_{\mu \nu} S_{\lambda \kappa} \tilde{\gamma}_{\nu s'_1 \kappa s'_2, \mu s_1 \lambda s_2}^2 \\ & + \frac{1}{4} \sum_{\nu \in A, \kappa \in B} \sum_{\mu \lambda} \sum_{j=x,y,z} \sum_{s_1 s'_1} \sum_{s_2 s'_2} \sigma_{s_1 s'_1}^j \sigma_{s_2 s'_2}^j S_{\mu \nu} S_{\lambda \kappa} \tilde{\gamma}_{\nu s'_1 \kappa s'_2, \mu s_1 \lambda s_2}^2, \end{aligned} \quad (10)$$

where a symmetrization was also carried out in order to obtain real values. Note that $\langle \hat{S}^2 \rangle = \sum_{AB} (\mathbf{S}_A \cdot \mathbf{S}_B)$.

3 Results and discussion

We present HF solutions of the generalized type for C_{84} (D_{6h}), C_{70} (D_{5h}), C_{60} (I_h), C_{36} (D_{6h}), C_{30} (D_{5h}), and for four isomers of C_{20} (the cage, the bowl, the ring, and a recently proposed pentagon structure [59]). We note that a D_2 and a D_{2d} isomer of C_{84} are known to be lower in energy than the D_{6h} structure considered in this work [60]. The features of the optimized geometries are described

in Sec. 3.1. In Sec. 3.2 we contrast the energies obtained by GHF with those from RHF. In Secs. 3.3, 3.4, and 3.5 we describe the polyradical character present in the GHF solutions in terms of the local magnetic moments, natural occupations, and atomic spin-spin correlation functions, respectively. Lastly, in Sec. 3.6 we provide a brief discussion on the interpretation of our results. In what follows, we provide a short review of the theoretical work on the smaller fullerenes.

The successful synthesis in 1998 of a solid form of C_{36} [61] prompted theoretical work on this fullerene [8, 62–66]. From early on it was recognized that the D_{6h} isomer possesses significant diradical character. After some disagreement in the geometry and even the multiplicity of the ground state, it was recognized that correlation effects play a very significant role in determining the correct geometry and electronic properties of this molecule [8]. Fewer theoretical studies have focused on C_{30} due to its triplet ground state character according to Hückel theory [67] and its observed low kinetic stability [68]. R(O)HF also predicts a triplet ground state for the D_{5h} structure [69].

Since the early days of fullerene science, C_{20} became an interesting subject for theoretical studies for at least two reasons: a) in order to understand the processes that drive the formation of C_{60} [70], and b) to determine what the smallest carbon cluster is for which a cage-like structure becomes the ground-state [71]. In particular, the C_{20} cage is the smallest possible fullerene that can be constructed out of only pentagon and hexagon rings: it has 12 pentagons (as required by Euler’s theorem) and no hexagons. After the realization that different methods predicted different stability patterns among the cage, ring, and bowl isomers [72–74], a large amount of theoretical work followed [75–81]. In 2000, Prinzbach *et al.* [82] reported the successful synthesis of the C_{20} fullerene cage from its perhydrogenated form. Later works helped to confirm the cage-like character of the reported structure [83, 84], or proposed further ways to characterize it [85, 86]. Some recent papers have established, using high-level correlated methods, the cage and the bowl to be nearly isoenergetic at zero temperature [87, 88]. Zhang, Sun, and Cao performed an extensive study of the Jahn-Teller distortions in the C_{20} cage [89]. We note the work of Heaton-Burgess and Yang [90], who have associated the delocalization error to the incorrect energetic ordering

predicted by density functional approximations. Using semi-empirical calculations, Greene and Beran [91] proposed a mechanism for the conversion between the ring and the bowl. The C_{20} cage has also been investigated [92–94] in the context of the Hubbard Hamiltonian, where it has become evident that electron correlation in the C_{20} cage plays a larger role than in its C_{60} counterpart.

3.1 Optimized geometries

Despite the many works in the literature studying the lowest-energy C_{20} isomers, relatively few of them have focused on the structural differences predicted by different *ab initio* methods. In a recent work, Grimme and Mück-Lichtenfeld [87] pointed out that the RHF/6-31G(*d*) structures considered by previous researchers might prove unreliable in order to obtain the correct energetic ordering with single-point correlated calculations. In particular, the geometries of the bowl and the cage were significantly changed when optimized with a correlated method. The authors ended up advocating the use of MP2 geometries obtained with a triple-zeta basis set.

We show in Fig. 1 the optimized GHF geometries for each of the four C_{20} isomers considered in this work. At the RHF level, the dodecahedral fullerene cage undergoes a first-order Jahn-Teller distortion yielding an optimized structure with reduced symmetry. Different authors have obtained different point groups for the optimized structure; we do not discard the possibility of there being several low-lying minima even at the RHF/6-31G(*d*) level. Our RHF/6-31G(*d*) calculations yielded a C_3 structure, with C-C bond distances in the range between 136.1 pm and 150.5 pm. On the other hand, GHF predicts a perfect dodecahedron (I_h symmetry), with all C-C bond distances equal to 147.1 pm. Re-optimizing the structures with the 6-311G(*d*) basis yielded only minimal changes, suggesting that they are well converged at the HF level. We note that Lin *et al.* [93] had already suggested that if electron correlation was strong enough in this system, the molecule would be stable against Jahn-Teller distortions. The GHF solution displays such character, as will be discussed in detail below.

The C_{20} bowl is predicted to have a C_{5v} configuration at the RHF level of theory, deviating from a planar structure. A similar geometry is also obtained with GHF. Nevertheless, RHF/6-

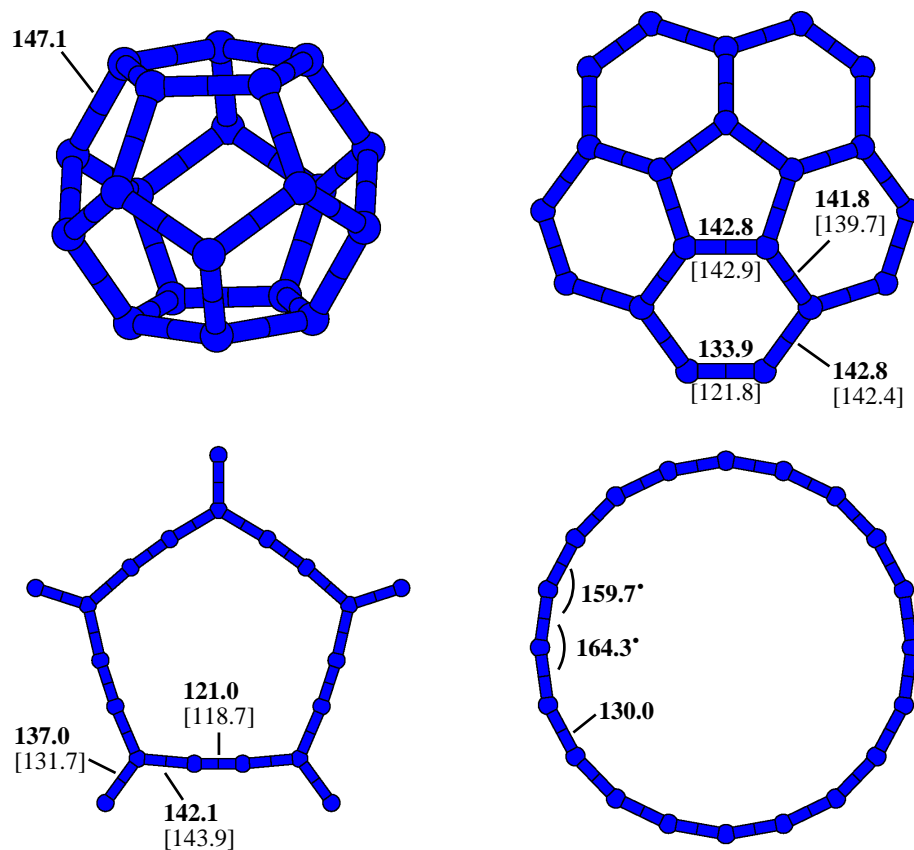


Figure 1: Structures of the four different C_{20} isomers considered in this work, with bond lengths given in pm optimized at the GHF/6-31G(*d*) level. The top left panel corresponds to the fullerene cage; GHF predicts a perfect dodecahedron with I_h symmetry. In the top right panel we show the bowl isomer (C_{5v}). The bottom left panel depicts the recently proposed [59] pentagon-like isomer (D_{5h}), while the bottom right panel shows the C_{20} ring isomer (D_{10h}). The latter is slightly deviated from a D_{20h} structure, as can be seen from the two different angles provided; all C-C distances are identical. For the bowl and pentagon isomers RHF/6-31G(*d*) bond lengths are also provided in brackets for comparison purposes.

31G(*d*) predicts a very short bond-length (121.8 pm) between the carbon atoms located in the edges of the bowl. GHF, on the contrary, yields a double-bond character between such atoms, with a much longer optimized bond distance (133.9 pm). Switching to the 6-311G(*d*) basis, the C-C bonds at the edges are shortened to 121.3 pm and 133.3 pm with RHF and GHF, respectively.

For the C₂₀ ring, RHF/6-31G(*d*) predicts a minimum with *C*_{10*h*} structure with alternating short (119.6 pm) and long (138.1 pm) bonds. The bonds are shortened to 119.1 pm and 137.7 pm upon enlarging the basis to 6-311G(*d*). GHF/6-31G(*d*), on the other hand, predicts a minimum with *D*_{10*h*} symmetry only slightly distorted from the ideal *D*_{20*h*} symmetry possible. In fact, all carbon-carbon bond lengths are predicted to be equivalent. Ten of the carbon atoms lie in a circumference with a radius of 416.6 pm, while the other ten atoms lie in a slightly smaller circle with radius of 414.0 pm. With the 6-311G(*d*) basis, GHF predicts a structure with perfect *D*_{20*h*} symmetry and C-C bond distances of 129.5 pm.

For the C₂₀ pentagon, both RHF and GHF predict, with the 6-31G(*d*) basis, the highly symmetric *D*_{5*h*} structure to be a true minimum. The two methods yield again a very large difference in the bond distance between the carbon atoms located in the corner of the pentagon (see Fig. 1). Both RHF and GHF predict, with the 6-311G(*d*) basis, slightly shorter bonds for the edge acetylenic and the corner C-C units.

We show in Fig. 2 the optimized geometries predicted at the GHF/6-31G(*d*) level for C₃₀ and C₃₆. It is noteworthy that, in both cases, GHF yields the fully symmetric geometry as a true minimum, whereas RHF (and even UHF) undergoes some form of Jahn-Teller distortion. The most notable difference between the GHF and RHF optimized structures for C₃₀ occurs in the capping pentagons. All C-C bonds are equivalent in GHF and possess a single-bond like character (146.0 pm), whereas RHF yields bond lengths with double- (135.1 pm) and single-bond character (147.6 pm). For C₃₆, both RHF and GHF predict structures with a *C*₆ axis of symmetry, though RHF only converges to a *C*_{6*v*} structure as opposed to the *D*_{6*h*} symmetry of the GHF structure. The carbon-carbon bonds in the capping hexagon are predicted to be significantly shorter by RHF (138.9 pm) than GHF (142.9 pm). We note that for both C₃₀ and C₃₆ the difference between the

GHF/6-31G(*d*) and GHF/6-311G(*d*) structures is minimal.

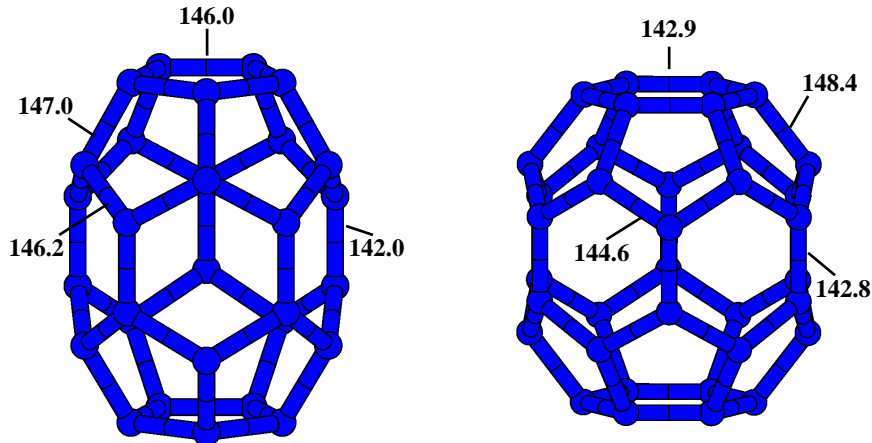


Figure 2: Structure of the C₃₀ (*D*_{5h}, left) and C₃₆ (*D*_{6h}, right) fullerene cages considered in this work. The GHF/6-31G(*d*) optimized geometries do not display any Jahn-Teller distortions to lower-symmetry structures.

For buckminsterfullerene (C₆₀) (not shown), both RHF/6-31G(*d*) and GHF/6-31G(*d*) predict an icosahedral geometry (*I*_h). The bond lengths predicted are significantly different, however. RHF predicts a short bond-length of 137.3 pm for hexagon-hexagon edges and a long bond-length of 144.9 pm for hexagon-pentagon edges. GHF, on the other hand, predicts longer carbon-carbon bonds of 140.7 pm and 145.2 pm, respectively, in good agreement with experimental gas-phase bond lengths [95]. These geometrical features are again preserved upon enlarging the basis to 6-311G(*d*). It is interesting to notice that the GHF predicted bond lengths are similar to those reported by Häser *et al.* at the MP2/TZP level [96].

For C₇₀ and C₈₄ (not shown), there are again significant structural differences between the RHF/6-31G(*d*) and the GHF/6-31G(*d*) optimized geometries. For instance, RHF yields bond lengths as short as 136.2 pm and as long as 147.2 pm for C₇₀. GHF, on the other hand, yields bond lengths in the interval 140.1–146.0 pm, displaying a tendency towards bond length equalization. For C₈₄, similar results are obtained: the mean bond lengths obtained with RHF and GHF are 142.3 and 143.5 pm, respectively, while the standard deviations are 3.5 and 2.1 pm.

We conclude that the HF geometries are, to a large extent, well converged with the 6-31G(*d*)

basis. The inclusion of spin-spin correlation effects (see below), even if only approximately at the GHF level, results in significant structural changes. Our GHF optimized geometries are still significantly different than the MP2/TZV2d1f ones reported in Ref. [87] for the cage, bowl, and ring isomers of C_{20} . Given the large static correlation present in these carbon clusters (see below), we find it more appropriate to optimize the geometries with either a multi-reference method or a broken-symmetry GHF-type independent-particle model.

3.2 Energetics

The energetic ordering between the ring, bowl, and cage isomers of C_{20} has been the subject of numerous previous works as discussed above. We present in Table 1 the total energies predicted with RHF, GHF, and S-GHF with a 6-31G(*d*) basis. It becomes immediately apparent that all methods agree in placing the pentagon significantly higher in energy than all other isomers.

Table 1: Total energies (in hartree, +756) predicted for the cage, bowl, ring, and pentagon isomers of C_{20} using the 6-31G(*d*) basis set. Relative energies (in eV) with respect to the ring isomer are shown in parentheses.

method	geom	cage	bowl	ring	pentagon
RHF	opt.	-0.556 79 (3.61)	-0.650 92 (1.05)	-0.689 48 (0.00)	-0.389 42 (8.17)
GHF	RHF	-0.698 56 (2.10)	-0.791 60 (-0.43)	-0.775 84 (0.00)	-0.417 77 (9.74)
GHF	opt.	-0.763 79 (3.12)	-0.871 28 (0.19)	-0.878 31 (0.00)	-0.430 89 (12.17)
S-GHF ($s = 0$)	GHF	-0.854 09 (3.43)	-0.979 49 (0.02)	-0.980 07 (0.00)	-0.566 44 (11.26)
S-GHF ($s = 1$)	GHF	-0.826 05	-0.946 74	-0.951 85	-0.491 61
S-GHF ($s = 2$)	GHF	-0.769 24	-0.903 28	-0.895 30	-0.410 60

RHF predicts the ring to be the most stable isomer, with the cage being 3.61 eV higher in energy. Using the RHF geometries, a huge energetic improvement is observed for all isomers upon allowing for symmetry breaking. GHF predicts the ring to be the most stable isomer using self-consistent geometries, though it is almost isoenergetic with the bowl. The cage is 3.12 eV higher in energy than the ring. We note that previous studies have predicted, using highly correlated approaches, the bowl and cage to be nearly isoenergetic with the ring being somewhat higher in energy [87, 88]. It would be interesting to repeat some of these calculations with the GHF

geometries reported in this work. All GHF solutions display significant spin contamination, with $\langle \hat{S}^2 \rangle$ equaling 6.42, 7.70, 7.23, and 5.14 a.u. for the cage, bowl, ring and pentagon isomers, respectively, at the GHF optimized geometries.

The energetic improvement afforded by S-GHF ($s = 0$) over GHF is significant in all cases, consistent with the large spin contamination observed in the GHF solutions. S-GHF predicts the triplet states of the cage, bowl, and ring isomers to lie ≈ 30 mhartree higher in energy than their singlet counterparts. The singlet-triplet gaps predicted by S-GHF are most likely overestimated, as the optimization of the wave function is naturally biased towards the ground state. Nonetheless, S-GHF clearly points towards a singlet ground state for all isomers. The quintet states are predicted to be significantly higher in energy in all cases.

In Table 2 we present a summary of the total energies and $\langle \hat{S}^2 \rangle$ predicted by RHF, UHF, and GHF for the larger fullerene systems. Several features are immediately apparent from the Table. The correlation energy (here defined as the difference with respect to the RHF energy) that GHF yields at the optimized geometries is huge in all cases, ranging from ≈ 160 mhartree for C_{60} to ≈ 280 mhartree for both C_{30} and C_{36} . Note that most of the energetic improvement is already recovered at the UHF level in C_{30} and C_{36} , but not in C_{60} , C_{70} , or C_{84} , where GHF still provides a significant improvement over UHF (50–60 mhartree). This is also reflected in the large difference in the spin contamination between UHF and GHF for the larger fullerenes. We point out that GHF should be preferred over UHF even for the smaller isomers in light of the highly symmetric structures that it affords and its ability to minimize spin frustration effects. As observed in the case of the C_{20} isomers, the energetic improvement brought upon by the geometry relaxation at the GHF level is significant. In other words, the difference between GHF//RHF and GHF//GHF energies is considerable in all cases. This is consistent with the large structural differences observed between RHF and GHF optimized geometries.

Table 3 displays the total energies predicted by S-GHF for the C_{30} and C_{36} fullerene cages, using the smaller 6-31G basis at the optimized GHF/6-31G(*d*) geometries. The singlet state is the lowest in energy, with the triplet state lying 24 and 31 mhartree above for C_{30} and C_{36} , respectively.

Table 2: Total energies (in hartree), molecular symmetries, and $\langle \hat{S}^2 \rangle$ (in a.u.) as predicted by RHF, UHF, and GHF for the C_{30} , C_{36} , C_{60} , C_{70} , and C_{84} fullerene cages. The 6-31G(*d*) basis was used in the calculations.

RHF//RHF			UHF//UHF			GHF//GHF			GHF//RHF
mol	sym	$\langle \hat{S}^2 \rangle$	E	sym	$\langle \hat{S}^2 \rangle$	E	sym	$\langle \hat{S}^2 \rangle$	E
C_{30}	C_s	0.00	-1135.187 47	C_2	7.66	-1135.467 13	D_{5h}	8.19	-1135.468 93
C_{36}	C_{6v}	0.00	-1362.540 56	D_{3h}	7.68	-1362.818 18	D_{6h}	8.12	-1362.826 72
C_{60}	I_h	0.00	-2271.830 39	C_i	7.52	-2271.925 54	I_h	10.26	-2271.991 34
C_{70}	D_{5h}	0.00	-2650.565 86	C_s	9.40	-2650.714 84	D_{5h}	12.09	-2650.769 31
C_{84}	D_{6h}	0.00	-3180.806 80	D_{3d}	11.62	-3181.007 10	D_{6h}	13.99	-3181.062 67

S-GHF thus agrees with multireference treatments for C_{36} in placing the singlet as the ground state [8]; the triplet ground state predicted by ROHF for C_{30} [69] is most likely incorrect.

Table 3: Total energies (in hartree) predicted by S-GHF for the C_{30} and C_{36} fullerene cages. The calculations were carried out with the 6-31G basis at the GHF/6-31G(*d*) optimized geometries.

method	C_{30}	C_{36}
GHF	-1135.022 96	-1362.302 35
S-GHF ($s = 0$)	-1135.129 03	-1362.434 33
S-GHF ($s = 1$)	-1135.105 25	-1362.403 55
S-GHF ($s = 2$)	-1135.057 66	-1362.346 75

3.3 Atomic magnetic moments

At this point, it is interesting to discuss the nature of the GHF solutions obtained for the various isomers. In particular, we shall investigate whether GHF predicts some type of torsional spin-density wave [42] being developed in the molecule. We note that the nature of the GHF solution for the C_{20} ring isomer (not shown) is truly collinear, anti-ferromagnetic in character, coinciding with a UHF-type description. In other words, an axial spin-density wave, with alternating up- and down-spins, develops along the ring.

Both the bowl and the pentagon C_{20} isomers display a non-collinear structure, as depicted in Fig. 3. In both isomers a torsional wave develops in order to minimize spin frustrations, even if

the nearest-neighbor interactions remain mostly anti-ferromagnetic in character. Interestingly, all the atomic moments in the bowl isomer are coplanar, with an enhanced spin density in the outermost carbon atoms. For the pentagon isomer, each acetylene-like unit along the edges has spins with a perfect anti-ferromagnetic alignment. Although the magnitudes of the magnetic moments displayed cannot be given a meaningful physical interpretation due to the known problems associated with the Mulliken population analysis [58], it is interesting that the magnetic moments in the pentagon isomer are $\approx 1/2$ in magnitude, the spin of a single electron. This is what one would expect if there was a single unpaired electron in a p orbital of each carbon atom.

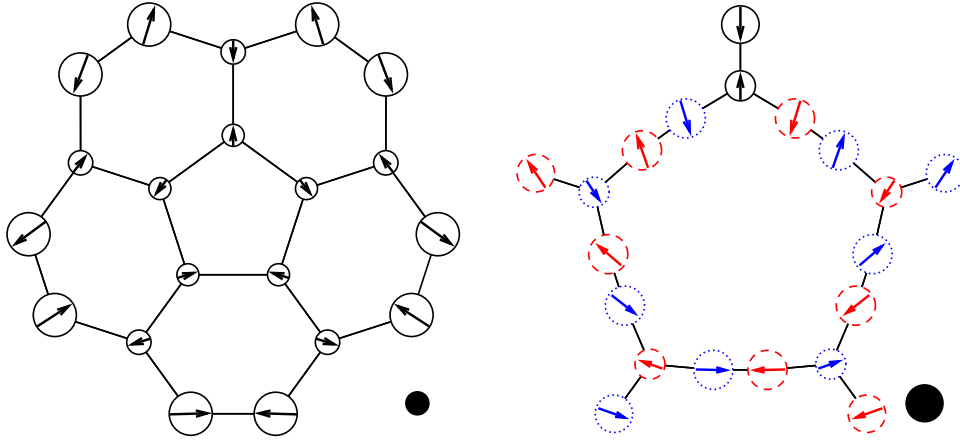


Figure 3: Atomic magnetic moments obtained from GHF/6-31G(d) calculations on the C_{20} bowl (left) and pentagon (right) isomers, at the optimized geometries. The *radius* of the circle is proportional to \mathbf{M}_A ; the filled black circle to the bottom-right sets the scale ($\mathbf{M}_A = 0.5$). In each center, the orientation of the xy -projection of \mathbf{M}_A is depicted as an arrow; if the z -projection is positive (negative), the circle is displayed as dashed-red (dotted-blue). A solid black circle was used to indicate that there is no z -projection: the atomic moment is fully oriented in the xy plane. Note that the absolute orientation of the atomic moments is unimportant (in non-relativistic calculations); it is only the relative orientation that determines the physics.

We show in Fig. 3 the atomic magnetic moments obtained from the GHF solution for the C_{20} cage at its optimized geometry. Our result is similar to that presented in Ref. [92] from the non-collinear HF solution of the C_{20} cage in a Hubbard Hamiltonian. Here, only the relative orientation of the moments is relevant. Each moment is oriented at an angle of $\approx 138^\circ$ with respect to its nearest neighbors, slightly deviating from the $4\pi/5$ angle that would yield coplanar spins in each pentagon. The structure thus obtained is the one that minimizes the frustration to the largest extent.

Note that all moments have exactly the same magnitude, $\approx 1/2$, which provides a rationalization for the perfectly symmetric optimized geometry obtained from GHF.

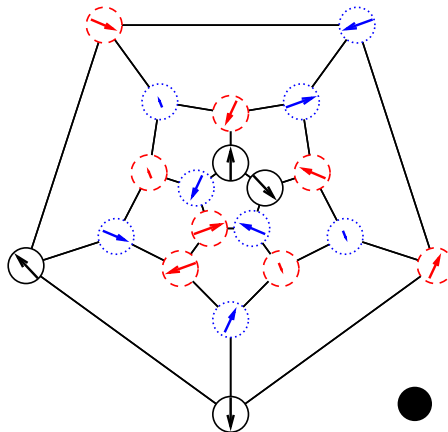


Figure 4: Same as Fig. 3, but for the C₂₀ fullerene cage, displayed as a Schlegel diagram.

We present, in Figs. 5 and 6, the atomic magnetic moments developed in GHF/6-31G(*d*) calculations of C₃₀, C₃₆, and C₆₀. As expected from the fact that the GHF solution does not coincide with UHF, all systems develop torsional spin density waves. The magnitude of the atomic magnetic moments is again $\approx 1/2$, suggesting the presence of a single unpaired electron.

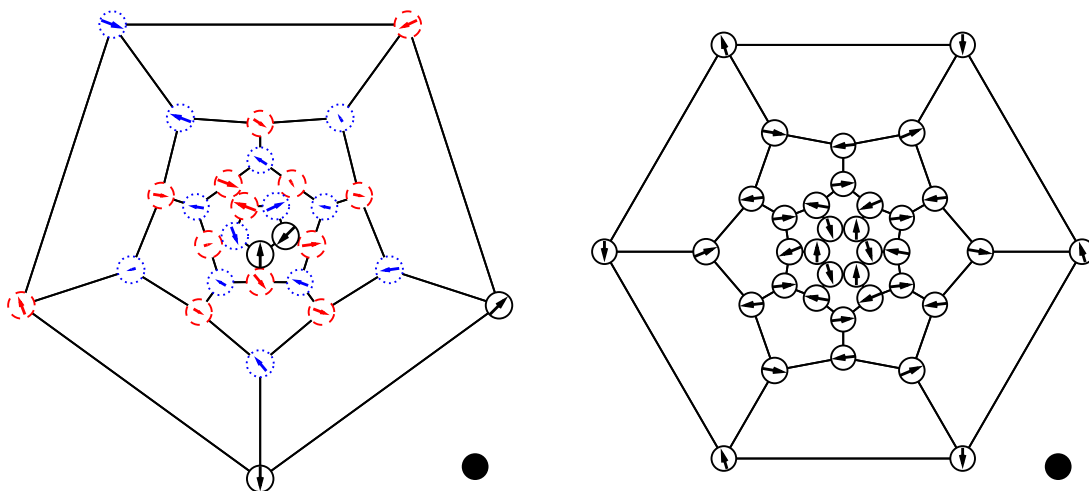


Figure 5: Same as Fig. 3, but for the C₃₀ (left) and C₃₆ (right) fullerene cages, displayed as Schlegel diagrams.

In C₃₀, each atomic moment in the capping pentagon (innermost and outermost pentagons) is

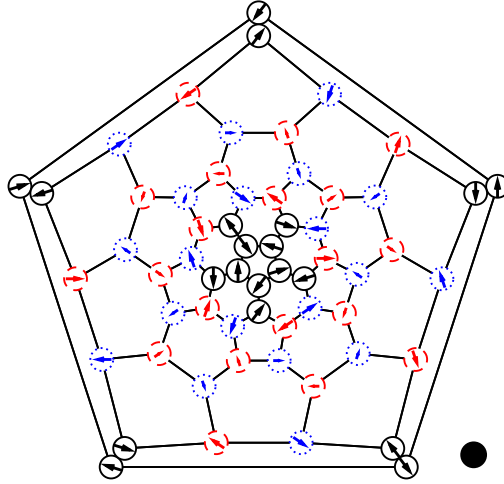


Figure 6: Same as Fig. 3, but for the C_{60} fullerene cages displayed as a Schlegel diagram.

oriented at an angle of $\approx 136^\circ$ with respect to its nearest neighbors, and at an angle of $\approx 70^\circ$ with respect to its next-nearest neighbors, thus minimizing spin frustration. In the hexagonal walls, we observe perfect anti-ferromagnetic interactions between those carbon atoms related by the mirror plane perpendicular to the C_5 axis of the molecule. In C_{36} , all the atomic magnetic moments lie in the same plane. In the capping hexagon, each moment is oriented at an angle of $\approx 165^\circ$ with respect to its nearest neighbors. The moment is parallel with respect to its next-nearest neighbors. Once again, we find exact anti-ferromagnetic pairing between those carbon atoms in the hexagonal walls related by the mirror plane perpendicular to the C_6 molecular axis.

For C_{60} , the spin arrangement coincides with that described by Coffey and Trugman [17] from the classical Heisenberg solution. This spin arrangement was also observed in the Hubbard solution for sufficiently large U/t (see, *e.g.*, Refs. [20, 28]). In particular, all spins in a given pentagon are coplanar, but spins in neighbor pentagons lie in a different plane. The normals to the spin planes in the pentagons are related in a non-trivial way. Perfect anti-ferromagnetic alignment between the carbon atoms defining the 6-6 bonds (hexagon-hexagon edges) is observed.

We show, in Fig. 7, the atomic magnetic moments obtained in GHF/6-31G(*d*) calculations in C_{70} and C_{84} . In C_{70} , the pentagons in the poles of the molecular structure have coplanar spins. The same is not true about other pentagons, which slightly deviate from this structure. The 5-6

bonds involving the carbon atoms in the poles display perfect anti-ferromagnetic alignment. The moments in the 6-6 bonds in the equatorial belt make an angle of $\approx 170^\circ$. In C_{84} , a perfect Néel type alignment is observed in the hexagons defining the poles. The spins in the equatorial belt also display perfect anti-ferromagnetic alignment.

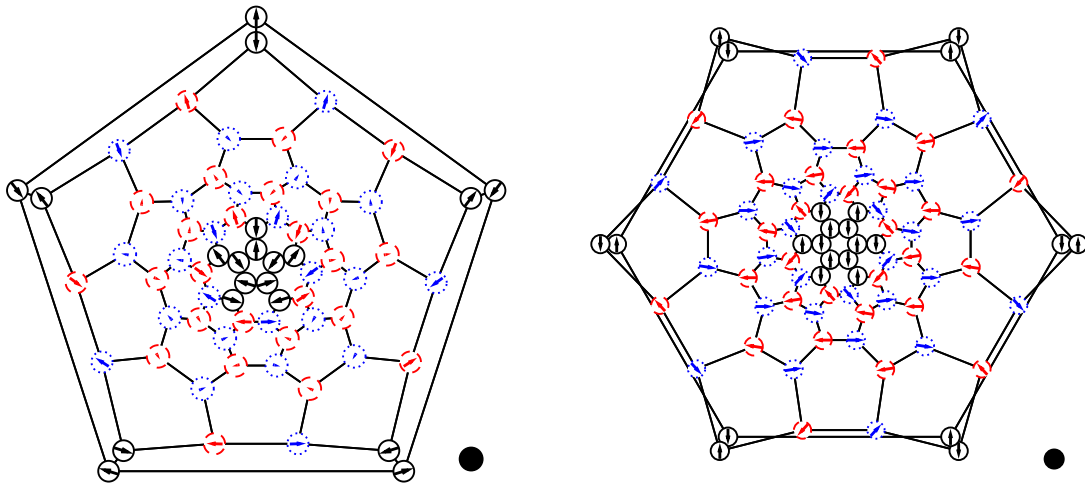


Figure 7: Same as Fig. 3, but for the C_{70} (left) and C_{84} (right) fullerene cages, displayed as Schlegel diagrams.

3.4 Natural occupations

One way to characterize the degree to which static correlation plays a role in a given system is to consider the natural occupation profile. If a (singlet) system is weakly correlated, all occupations are expected to remain close to zero or two. Conversely, occupation numbers near one signal the failure of (restricted) HF to become an accurate zero-th order wave function: several determinants contribute nearly equally to the exact wave function expansion.

We present in Fig. 8 the charge natural occupations obtained by diagonalizing the charge density matrix $P_{V\mu} = \sum_s \gamma_{Vs,\mu s}^1$ associated with the GHF solution for each of the four C_{20} isomers under consideration. This is equivalent to the well-known procedure to obtain the natural orbitals and natural occupations from UHF wave functions [97]. Additionally, we present the natural occupations (as true eigenvalues of the density matrix) obtained after carrying out the (singlet) spin-projection

from the GHF wave function.

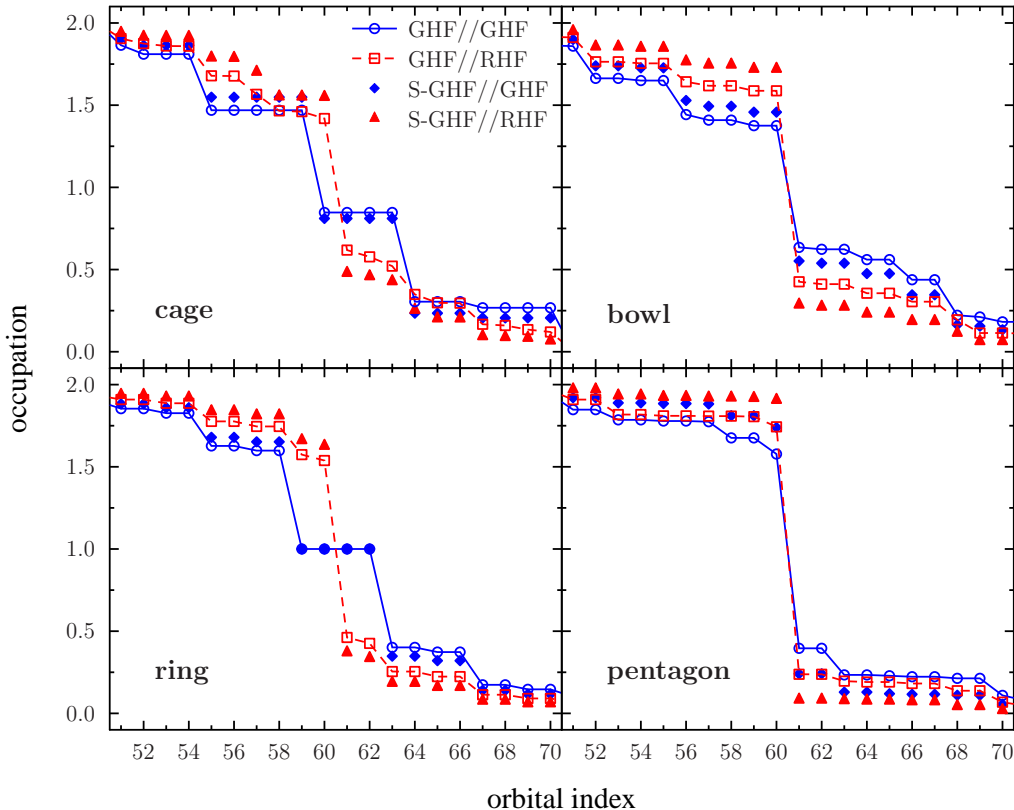


Figure 8: Natural occupations predicted by S-GHF ($s = 0$) and charge natural occupations predicted by GHF for each of the four C_{20} isomers considered in this work, at the optimized RHF and GHF geometries. The 6-31G(d) basis was used; only the occupations in the π -space are depicted.

From Fig. 8, one immediately realizes that the GHF charge natural occupations become closer to one at the GHF geometries (as compared to the RHF ones). This is a consequence of the bond length equalization observed in GHF optimized geometries, as opposed to the alternating double- and single-bond character predicted by RHF. It is also evident from the figure that S-GHF reduces the amount of static correlation predicted by GHF, as occupation numbers become closer to zero and two with the former, more accurate method. The inclusion of dynamical correlation may contribute to this effect even further. Aside from these generic trends, we see marked differences between the four C_{20} isomers. The C_{20} pentagon displays few signatures of static correlation, and may be accurately treated by single-reference based methods. The bowl, cage, and ring isomers do display features of static correlation, with several occupations between 0.4 and 1.6. An accurate

description of the electron correlation in such systems would require either a multi-reference or a symmetry-broken based treatment. In particular, the ring isomer displays four occupations ≈ 1 (they become exactly one for a D_{20h} geometry). These orbitals are thus singly occupied, though entangled in an overall singlet wave function for S-GHF.

We show in Fig. 9 the charge natural occupations predicted by GHF and the natural occupations predicted by S-GHF ($s = 0$) for C_{30} and C_{36} , evaluated at the optimized GHF geometries. As observed in the isomers of C_{20} , S-GHF reduces the apparent amount of static correlation predicted by GHF, bringing the occupations closer to 0 or 2 (albeit only slightly). Both C_{30} and C_{36} can be immediately characterized as possessing large static correlation, as already observed in the literature for C_{36} [8, 63]. In particular, they both display a few occupations near 1.

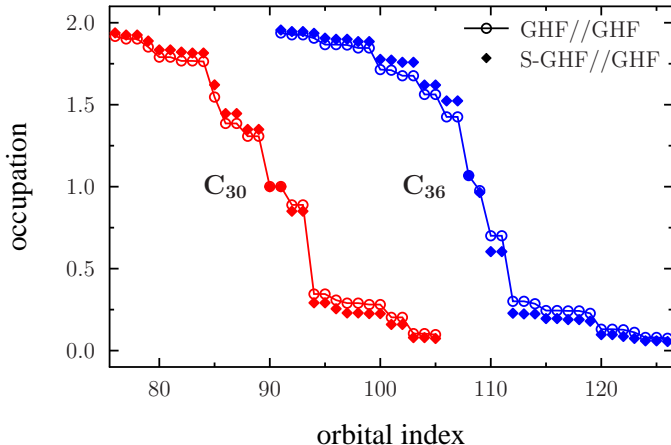


Figure 9: Same as Fig. 8, but for the C_{30} and C_{36} fullerene cages.

Fig. 10 shows the natural occupations in C_{60} , C_{70} , and C_{84} . In all of these cases we observe a significant gap in the occupation numbers, although the gap is reduced for the two larger cages. In C_{60} , for instance, S-GHF predicts no occupation in the range $0.6 < n < 1.4$. Nevertheless, we would argue that the profiles are still far from being single-determinantal in nature. We note that the C_{60} GHF occupation profile displays more static correlation than that reported with UHF by Stück *et al.* [7] as there are more orbitals with occupation in the range $0.4 < n < 1.6$. We anticipate that single-reference based methods (especially of the coupled-cluster type), can be significantly more successful in C_{60} , C_{70} , or C_{84} than in either C_{30} or C_{36} .

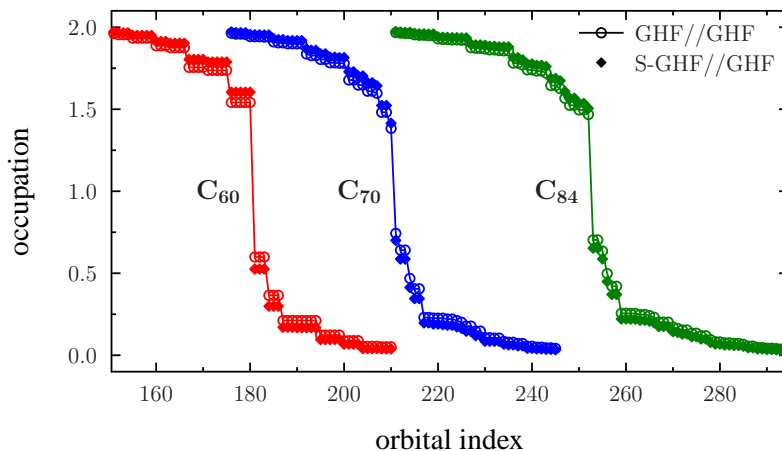


Figure 10: Same as Fig. 8, but for the C_{60} , C_{70} , and C_{84} fullerene cages.

Overall, the occupation profiles displayed for the fullerene isomers are consistent with a polyradical character. The effective number of unpaired electrons can be quantified using empirical formulas such as that proposed by Head-Gordon [98],

$$N_{\text{unpaired}} = \sum_i \min(n_i, 2 - n_i). \quad (11)$$

S-GHF/6-31G(*d*) calculations, at the optimized GHF geometries, predicts 10.2, 8.8, and 9.9 unpaired electrons in C_{30} , C_{36} , and C_{60} , respectively. This increases to 12.4 and 14.5 for C_{70} and C_{84} . The large polyradical character displayed by the fullerenes rationalizes their increased reactivity as compared to typical aromatic systems.

3.5 Spin-spin correlations

Having observed that GHF predicts magnetic moments in each carbon center and that such structure is intrinsically connected with the development of static correlation, the next thing is to establish the nature of the interactions between the magnetic moments. In particular, we study the inter-atomic spin-spin correlations using Eq. ??.

We begin by considering the C_{20} ring, for which GHF predicts an axial spin-density wave character. We show in Fig. 11 the atomic spin-spin correlations predicted by RHF/6-31G(*d*)

and GHF/6-31G(*d*) at the corresponding optimized geometries. In RHF, the magnetic moment (or spin) in each atom is strongly (negatively) correlated with its doubly-bonded neighbor, and weakly with its singly-bonded neighbor. Note that the RHF structure does not follow an anti-ferromagnetic pattern. GHF, on the other hand, displays long-range spin-spin correlations, as shown in the right panel. That is, if the spin in the probe atom is up, one can know *a priori* the spins in all other atoms, due to the anti-ferromagnetic character of the spin density wave. This type of structure can be explained in terms of strong nearest-neighbor-type spin-spin interactions between the singly occupied *p* orbital in each carbon atom, exactly those considered in model Hamiltonian approaches.

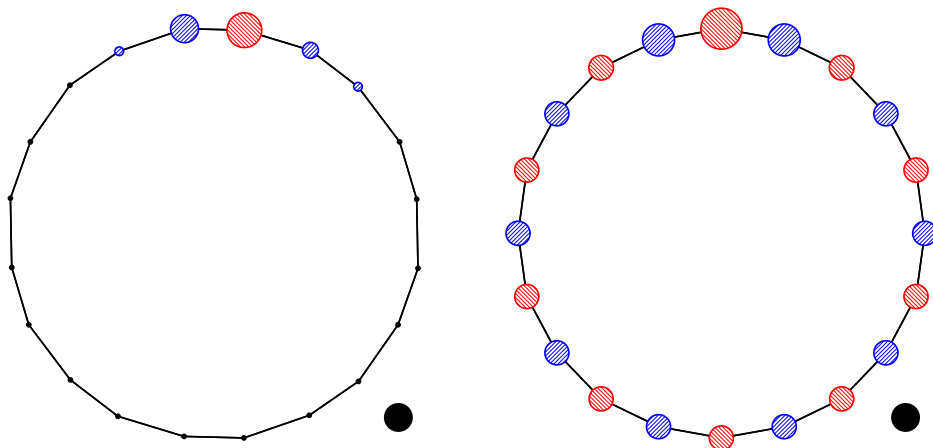


Figure 11: Atomic spin-spin correlations in the RHF/6-31G(*d*) (left panel) and GHF/6-31G(*d*) (right panel) solutions of the C_{20} ring, at the corresponding optimized geometries. A red (blue) circle indicates a positive (negative) correlation; the *area* of the circle is proportional to the magnitude of the correlation. The atom with the largest red circle (near the top of the figure) is used as probe. The black circle located at the bottom right of each figure is used to set the scale ($\mathbf{S}_A \cdot \mathbf{S}_B = 1$).

We note that only the relative magnitudes of the atomic spin-spin correlations should be given physical meaning. The fact that the on-site spin-spin correlation is significantly larger than $3/4$ can be attributed to contributions from the σ -bonded electrons.

The same type of behavior is observed in other isomers. We show in Fig. 12 the atomic spin-spin correlations in the C_{20} bowl isomer, using an atom in the edge as a probe. Again, RHF predicts strong correlations only with its triply-bonded neighbor. On the other hand, GHF predicts strong correlations of long-range character.

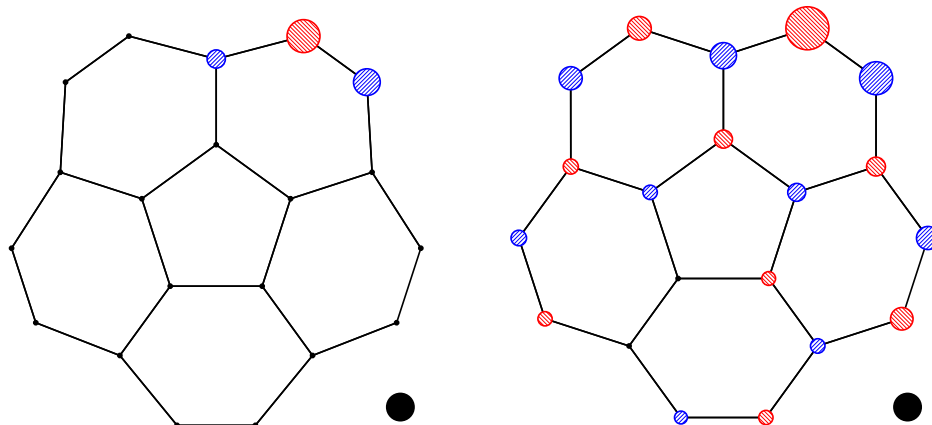


Figure 12: Same as Fig. 11, but for the bowl isomer of C_{20} ; the probe atoms are located near the top-right corner of the figure. The left panel corresponds to the RHF solution, while the right displays the GHF solution.

To show that GHF still predicts a strongly correlated nature between localized spins in C_{60} , we show in Fig. 13 the atomic spin-spin correlations in this molecule predicted by RHF and GHF. The RHF solution predicts that there are significant spin-spin correlations between the carbon center and its three nearest neighbors. GHF yields the same type of strong correlations, but it also displays non-vanishing spin-spin correlations with most other atoms in the fullerene lattice. The nature of the GHF electronic wave function is thus polyradical in character. We note that the ratio of the magnitudes of the spin-spin correlations between the 6-5 and 6-6 bonds is 0.86, significantly larger than the ratio obtained from accurate solutions to the Heisenberg Hamiltonian [99]. A large part of this effect is, nevertheless, due to contributions from σ -bonded electrons.

For C_{70} (not shown) and C_{84} (see Fig. 14), we again observe the development of long-range anti-ferromagnetic ordering. Interestingly, it appears that the atomic spin-spin correlations are separately enhanced in the equator and the poles of the molecules.

In Ref. [7], Stück *et al.* concluded that there is no strong correlation present in C_{60} according to the occupation profile predicted by UHF and optimized scaled opposite-spin MP2, and the fact that RHF-based MP2 predicted a more accurate singlet-triplet gap than UHF-based calculations. They interpreted the spin symmetry breaking occurring in C_{60} as due to relatively small but global electron correlations in the π -space, in spite of the large spin density with anti-ferromagnetic char-

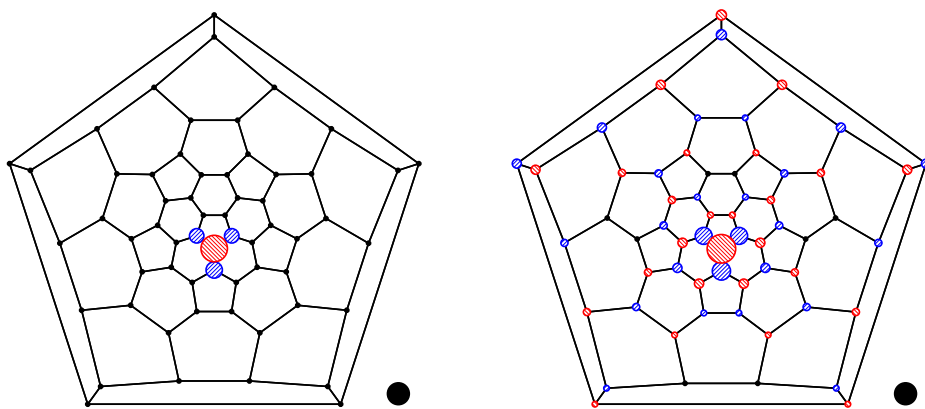


Figure 13: Same as Fig. 11, but for the C_{60} fullerene cage shown as a Schlegel diagram, with the probe atoms located near the center of the structure. The left panel corresponds to the RHF solution, while the right displays the GHF solution.

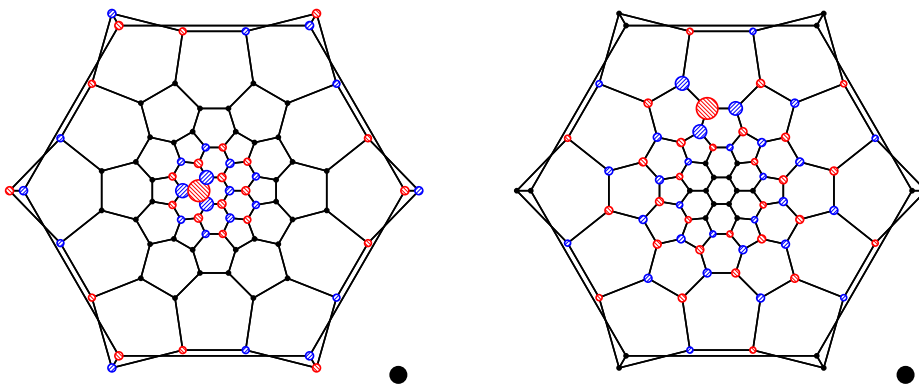


Figure 14: Same as Fig. 11, but for the C_{84} (D_{6h}) fullerene cage shown as a Schlegel diagram. Only the GHF solution is displayed, with the probe atom located in the pole (left panel) or in the equator (right panel) of the molecule.

acter. Our results support a different interpretation, one where the system is strongly correlated in the sense that short-range spin-spin interactions drive long-range magnetic ordering. This is more consistent with the nature of valence bond solutions to the Heisenberg Hamiltonian [34] and with accurate Monte-Carlo results to the Hubbard Hamiltonian (see, *e.g.*, Ref. [22]). GHF predicts the correct qualitative physical picture, though quantitative agreement with the exact solution can only be obtained with correlated approaches.

3.6 Discussion

Previous works have related the observed large spin contamination in independent-particle model wave functions (HF and DFT) to the concept of polyradicalism [100]. At this point, this relation seems transparent in fullerene and related systems (such as polyacenes): the large spin contamination in symmetry broken approaches appears due to large atomic spin-spin correlations. The latter are in turn a result of spins being partially localized in the carbon centers so as to maximize anti-ferromagnetic interactions (including minimizing the inherent frustration present in the system).

One must ask whether the physical picture portrayed by these solutions is correct. We find three problems with GHF solutions that one must keep in mind:

- GHF predicts non-zero atomic magnetic moments on the atoms, with the spins aligned according to a pattern that minimizes frustration. This is an *unphysical* effect for a true singlet solution, where the average net spin density should identically vanish over all space. In other words, the correct description should have *fluctuating* spins, as opposed to the *permanent* spins in broken symmetry approaches, that yield a net zero magnetization at every point in space.
- The GHF solution displays a large spin contamination. In other words, the sum over the atomic spin-spin correlations results in a non-zero value for a singlet state.
- The broken-symmetry GHF solution predicts long-range ordering of the spins. The magni-

tude of the spin-spin correlation is roughly the same for, say, the third neighbor than for a far-away neighbor, as seen for the C_{20} ring.

The first two problems can be easily fixed by spin-projection of the optimized GHF wave function. S-GHF predicts a zero atomic magnetic moment on each atom, and the sum of the inter-atomic spin-spin correlations identically vanishes for singlet states.

The third effect is more subtle, although broken symmetry HF tends to overemphasize the long-range correlations. We illustrate this by comparing the spin-spin correlations in the C_{20} ring with those from a 24-site periodic $s = 1/2$ Heisenberg chain, as shown in Fig. 15. Whereas RHF fails to produce any type of magnetic ordering, GHF overemphasizes the strength of the long-range spin-spin correlations. The spin-spin correlations are known to decay as $\sim \log^\sigma r/r$ in one-dimensional spin chains, with $\sigma \approx 0.5$ [101, 102]. The spin-spin correlations also display long-range ordering with a power law decay in one-dimensional Hubbard chains (see, *e.g.*, Refs. [103, 104]). It is clear from the figure that a simple projection-after-variation spin projection does not change the long-range character of the GHF correlations; it simply reweighs some of the values so that the sum adds up to zero (for a singlet state). We note that if a re-optimization of the orbitals is allowed (in a variation-after-projection scheme), S-GHF may change the structure of the spin-spin correlations by introducing defects into the Slater determinant (see Fig. 15).

For highly symmetric systems, one can gain a clearer insight to the inter-atomic spin-spin correlations by decomposing them into the different irreducible components. This is commonly done in periodic systems and was also done by Srinivasan and co-workers [26] for C_{60} , which lead them to conclude that the spin structure has large weights in the T_{2g} and G_u representations. We find it more convenient to introduce simple measures of the strength of the overall spin-spin

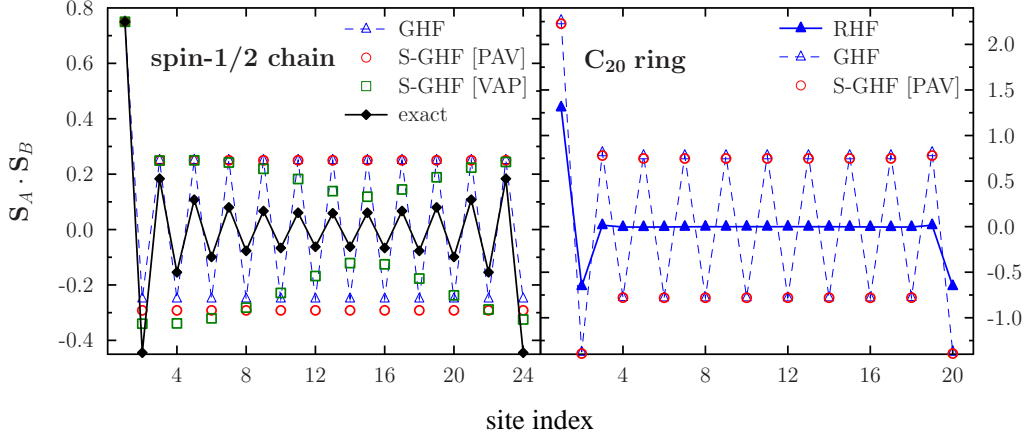


Figure 15: Spin-spin correlations predicted by HF and symmetry-projected HF in a 24-site spin-1/2 periodic Heisenberg chain (left) and in the C_{20} ring (right). For the C_{20} ring, the calculations use the 6-31G(*d*) basis set and were carried out at the GHF/6-31G(*d*) optimized geometries. PAV and VAP denote projection-after-variation and variation-after-projection calculations. The latter implies a re-optimization of the orbitals in the presence of the projection operator. The exact results for the spin-1/2 periodic chain are from Ref. [101].

correlations and the “long-range” part of them. Namely, we introduce the following measures:

$$\langle S^2 \rangle = \sum_{AB} \mathbf{S}_A \cdot \mathbf{S}_B, \quad (12)$$

$$\langle S^2 \rangle_{\text{abs}} = \frac{1}{N_A} \sum_{AB} |\mathbf{S}_A \cdot \mathbf{S}_B|, \quad (13)$$

$$\langle S^2 \rangle_{\text{abs,lr}} = \langle S^2 \rangle_{\text{abs}} - \frac{1}{N_A} \sum_A |\mathbf{S}_A \cdot \mathbf{S}_A| - \frac{2}{N_A} \sum_{\langle AB \rangle} |\mathbf{S}_A \cdot \mathbf{S}_B|. \quad (14)$$

Whereas $\langle S^2 \rangle$ should sum to zero for a singlet state, $\langle S^2 \rangle_{\text{abs}}$ measures the overall strength of the spin-spin correlations by summing the absolute values of the inter-atomic interactions. The normalization factor $1/N_A$ is introduced for convenience. If long-range order is present in a class of systems, we expect $\langle S^2 \rangle_{\text{abs}}$ to scale linearly with the size of them. $\langle S^2 \rangle_{\text{abs,lr}}$ measures the “long-range” part of the interactions by subtracting the on-site and the nearest-neighbor correlations from $\langle S^2 \rangle_{\text{abs}}$.

We have computed these three quantities for the systems under consideration; the results are presented in Table 4. Neither RHF nor S-GHF present any spin contamination. The RHF wave

functions introduce almost no long-range spin-spin correlations, as we had pointed out before in the figures, and give almost constant values for $\langle S^2 \rangle_{\text{abs}}$. On the other hand, both GHF and its spin-projected version introduce magnetic ordering in the systems which becomes reflected in large $\langle S^2 \rangle_{\text{abs}}$ and $\langle S^2 \rangle_{\text{abs,lr}}$ values. The largest values observed are for the C₂₀ ring, which is unsurprising given the axial character of the spin density wave. For the fullerene cages, $\langle S^2 \rangle_{\text{abs}}$ and its long-range counterpart increase with the size of the system, but they do so in a sub-linear way. This can be understood from the fact that the geometric structures of the cages have different nature (in terms of adjacent pentagons and hexagons) and the frustration included in the various cages has different character.

Table 4: Computed measures of the strength of spin-spin correlations as given by Eqs. ??, ??, and ?? for different systems. The 6-31G(*d*) basis set was used.

system	RHF//RHF			GHF//GHF			S-GHF//GHF		
	$\langle S^2 \rangle$	$\langle S^2 \rangle_{\text{abs}}$	$\langle S^2 \rangle_{\text{abs,lr}}$	$\langle S^2 \rangle$	$\langle S^2 \rangle_{\text{abs}}$	$\langle S^2 \rangle_{\text{abs,lr}}$	$\langle S^2 \rangle$	$\langle S^2 \rangle_{\text{abs}}$	$\langle S^2 \rangle_{\text{abs,lr}}$
C ₂₀ bowl	0.00	2.97	0.05	7.70	9.42	4.92	0.00	9.40	4.85
C ₂₀ ring	0.00	3.02	0.16	7.23	18.33	13.22	0.00	18.05	12.94
C ₂₀ cage	0.00	2.91	0.09	6.42	5.88	2.21	0.00	5.91	2.18
C ₃₀ cage	0.00	2.91	0.08	8.19	7.76	4.03	0.00	7.71	3.96
C ₃₆ cage	0.00	2.96	0.10	8.12	8.53	4.85	0.00	8.35	4.66
C ₆₀ cage	0.00	2.98	0.08	10.26	9.22	5.61	0.00	8.98	5.38
C ₇₀ cage	0.00	2.98	0.08	12.09	11.20	7.54	0.00	10.94	7.29
C ₈₄ cage	0.00	2.99	0.08	13.99	14.46	10.78	0.00	14.12	10.45

At this point, we can state what one expects from highly accurate correlated calculations. $\langle S^2 \rangle_{\text{abs}}$ should be much larger than in RHF but is likely going to be significantly smaller than in GHF. The near zero value predicted by RHF for $\langle S^2 \rangle_{\text{abs,lr}}$ is most certainly qualitatively incorrect. Indeed, highly accurate quantum Monte Carlo calculations [22] in the C₆₀ Hubbard lattice have shown that spin correlations vanish at *large* distances, with a correlation length of 3-4 bonds. Density-matrix renormalization group (DMRG) calculations of Hachmann and coworkers in polyacene systems [35] have also displayed magnetic ordering but with decaying spin-spin correlations.

The nature of the chemical bond in large conjugated molecules becomes dominated by short-range spin-spin type interactions. This is in contrast to the delocalized, non-interacting electron-gas

picture offered by Hückel theory. We agree with Hachmann *et al.* [35] and Schmalz [34] on the fact that the bonding is most simply expressed in terms of a valence bond framework. Ionic contributions (zero and double occupations) in the π -orbitals are diminished in favor of a resonating valence bond structure between the localized electrons in each carbon center. The system becomes a Mott insulator [105], rather than displaying metallic-like behavior. This is likely true regardless of the shape of the molecule (fullerene, graphene-like ribbon, carbon nanotube, etc.). A broken symmetry HF approach is consistent with this framework, but predicts too much magnetic ordering. Ionic contributions are however, still significant, as can be seen from the occupation profiles displayed above. Although the occupations are far from zero or two, they are clearly also far from being all identical to one. We thus expect that a Heisenberg-type Hamiltonian can only offer a qualitative picture of the nature of the spin-spin interactions. The Hubbard and the Pariser-Parr-Pople model Hamiltonians are more appropriate to understand the electron correlation in the π -space of conjugated systems such as the fullerenes.

We note that the charge natural occupation profiles obtained in GHF calculations are possibly useful in parametrizing Hubbard-type Hamiltonians for fullerenes. Here, the Hubbard Hamiltonian is written in the form

$$\hat{H} = - \sum_{ij} t_{ij} \sum_{s=\uparrow,\downarrow} \left(c_{i,s}^\dagger c_{j,s} + c_{j,s}^\dagger c_{i,s} \right) + U \sum_i n_{i,\uparrow} n_{i,\downarrow}, \quad (15)$$

where i, j label lattice sites in the fullerene, and t and U correspond to hopping (kinetic energy) and on-site (Coulomb) repulsion amplitudes, respectively. In particular, the charge natural occupations predicted by GHF approximations in both the Hubbard Hamiltonian and the *ab initio* system can be used in a least-squares fit sense (see Fig. 16). The fact that the Hubbard Hamiltonian parameters are adjusted so that an approximate method yields similar results is appealing.

The use of this strategy for the C_{20} fullerene cage results in $U/t \sim 4.2$ when only nearest-neighbor hopping is used. This places the fullerene in the intermediate-to-strong correlated regime (considering that the single-particle bandwidth is $\approx 6t$). As shown in Fig. 16, the GHF charge

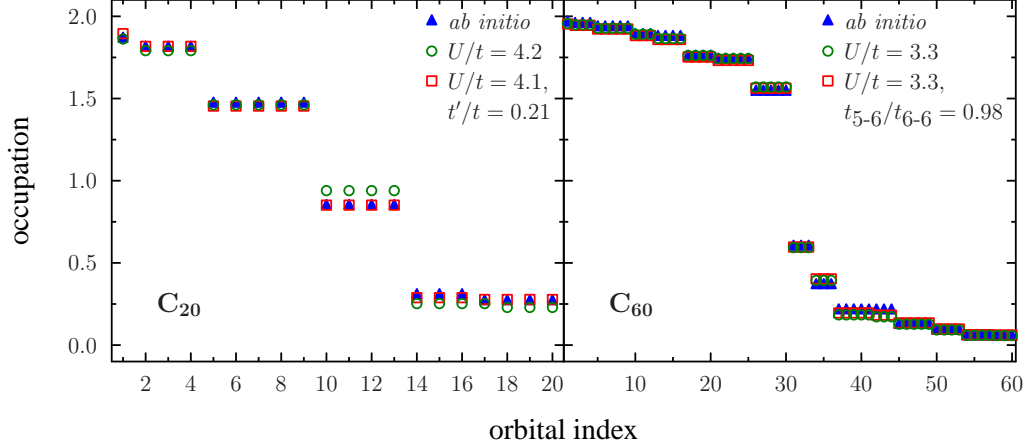


Figure 16: Comparison of GHF charge natural occupations predicted from the *ab initio* results and Hubbard Hamiltonian parametrizations for the C_{20} (left) and C_{60} (right) fullerene cages. More details are provided in the main text.

natural occupation profile obtained from the Hubbard-type Hamiltonian resembles well the *ab initio* one, save for the lowest-occupied states. A better fit can be obtained using an additional next-nearest-neighbor hopping amplitude $t'/t \sim 0.21$ and $U/t \sim 4.1$.

For the C_{60} fullerene cage, assuming homogeneous hopping parameters and only nearest-neighbor hopping allowed, one obtains $U/t \sim 3.3$. As we have previously discussed, the electron correlation in C_{60} is weaker than in C_{20} , so this is unsurprising. The charge natural occupation profile from the Hubbard Hamiltonian is in fairly good agreement with the *ab initio* one. We obtain a slightly better fit by allowing different hoppings in the 5-6 bonds than in the 6-6 bonds: $t_{5-6}/t_{6-6} \sim 0.98$, with $U/t \sim 3.3$.

We note that our U/t value for C_{60} is well within the range $2 \leq U/t \leq 5$ considered by other works [20–22, 24–26, 28, 30]. Our parametrization for U/t for C_{20} is significantly smaller than that reported by Lin and Sørensen [94]. The need for next-nearest neighbor hopping in the latter lattice might be understood in terms of the larger s character of the hybridized orbitals defining the π -space in C_{20} than in C_{60} , due to the higher curvature of the structure. We plan to study in the near future the extent to which simple Hubbard-type parametrizations reproduce the low-energy physics of selected fullerene cages.

4 Conclusions

In this work, we have shown a few examples of fullerene systems where HF solutions of the generalized type (with non-collinear spin arrangements) are lower in energy than their respective restricted counterparts. In these solutions, effective localized magnetic moments develop in the p orbitals of each carbon center; the spins become aligned in such a way so as to maximize anti-ferromagnetic interactions and minimize frustration. The large spin contamination observed in these solutions is indicative of strong inter-atomic spin-spin correlations that should determine the low-energy physical and chemical properties of fullerenes. The GHF-based optimized geometries avoid Jahn-Teller type distortions in fullerene cages such as C_{20} , C_{30} or C_{36} . Fullerene molecules are predicted to be polyradical in nature and thus either a multi-reference or a broken symmetry treatment is necessary to get a correct qualitative physical picture.

It would be interesting to tackle some of the examples here considered with more accurate multi-reference based methods in order to obtain a complete picture of the nature of the electronic structure in fullerenes and of the importance of spin-spin correlations in particular. Unfortunately, large active spaces seem inevitable (due to the size of the systems and the fact that σ -orbitals cannot be completely ignored). This would also permit to assess the extent to which model Hamiltonians describe the properties of fullerene systems (see, *e.g.*, Refs. [34, 106]) or, equivalently, the extent to which the π -space is fully responsible for low-energy electronic properties. We note that the radical scavenger character of C_{60} [4] suggests that spin-spin correlations are indeed significant. An interesting alternative avenue is to explore non-collinear density functional-based approaches for the fullerenes (see, *e.g.*, Ref. [107]).

We think it would also be interesting to re-investigate some of the chemical properties of fullerenes with GHF-based solutions as opposed to the traditional restricted framework adopted either in HF or density functional approaches. In particular, we are interested in the extent to which spin-spin correlations account for the observed addition patterns in fullerene reactions. Further investigations can also explore how the spin structure is affected by incarcerated species or by defects in the fullerene structure such as the introduction of edges. The study of fullerene

analogues such as boron-nitride, silicon, or germanium-based structures is also appealing.

Aside from that, we believe that fullerenes may become model systems in which, on the one hand, both model Hamiltonian and full *ab initio* calculations can be carried out, and, on the other, actual experiments can be performed. Given that doping is believed to be a precursor for superconductivity in Mott-insulating environments, it would be interesting to study the electronic structure of doped systems, both by ionization and by chemical means. (We note that chemists have been successful in preparing heterofullerenes [4] where, *e.g.*, a carbon atom is replaced by an electron-doped nitrogen atom or a hole-doped boron center.)

More generally, we believe that broken symmetry HF approaches can help to understand the nature of the chemical bonding in other carbon-based structures such as carbon nanotubes or graphene-like structures. The recent work by Sheka and Chernozatonskii following this idea should be highlighted [108–110]. The spin symmetry-projection strategy is important in order to eliminate the unphysical effects in these solutions.

Acknowledgement

This work was supported by the National Science Foundation (CHE-1110884). G.E.S. is a Welch Foundation Chair (C-0036). Some of the computational resources used were provided in part by NIH award NCRR S10RR02950 and an IBM Shared University Research (SUR) award in partnership with CISCO, Qlogic and Adaptive Computing.

References

- (1) Kroto, H. W.; Heath, J. R.; O’Brien, S. C.; Curl, R. F.; Smalley, R. E. *Nature* **1985**, *318*, 162–163.
- (2) Heath, J. R.; O’Brien, S. C.; Zhang, Q.; Liu, Y.; Curl, R. F.; Tittel, F. K.; Smalley, R. E. *J. Am. Chem. Soc.* **1985**, *107*, 7779–7780.

- (3) Krätschmer, W.; Lamb, L. D.; Fostiropoulos, K.; Huffman, D. R. *Nature* **1990**, *347*, 354–358.
- (4) Taylor, R. *Lecture Notes on Fullerene Chemistry: A Handbook for Chemists*; Imperial College Press: London, 1999.
- (5) Scuseria, G. E. *Science* **1996**, *271*, 942–945.
- (6) Paulus, B. *Int. J. Quantum Chem.* **2004**, *100*, 1026–1032.
- (7) Stück, D.; Baker, T. A.; Zimmerman, P.; Kurlancheek, W.; Head-Gordon, M. *J. Chem. Phys.* **2011**, *135*, 194306.
- (8) Varganov, S. A.; Avramov, P. V.; Ovchinnikov, S. G.; Gordon, M. S. *Chem. Phys. Lett.* **2002**, *362*, 380–386.
- (9) Sheka, E. F. *Int. J. Quantum Chem.* **2004**, *100*, 375–387.
- (10) Sheka, E. F. *J. Struct. Chem.* **2006**, *47*, 593–599.
- (11) Sheka, E. F. *Int. J. Quantum Chem.* **2007**, *107*, 2803–2816.
- (12) Sheka, E. F.; Razbirin, B. S.; Nelson, D. K. *J. Phys. Chem. A* **2011**, *115*, 3480–3490.
- (13) Sheka, E. *Fullerenes. Nanochemistry, Nanomagnetism, Nanomedicine, Nanophotonics*; CRC Press: Boca Raton, 2011.
- (14) Sheka, E. F. *Int. J. Quantum Chem.* **2004**, *100*, 388–406.
- (15) Sheka, E. F. *Chem. Phys. Lett.* **2007**, *438*, 119–126.
- (16) Taylor, R.; Hare, J. P.; Abdul-Sada, A. K.; Kroto, H. W. *J. Chem. Soc., Chem. Commun.* **1990**, 1423–1425.
- (17) Coffey, D.; Trugman, S. A. *Phys. Rev. Lett.* **1992**, *69*, 176–179.

- (18) Konstantinidis, N. P. *Phys. Rev. B* **2005**, 72, 064453.
- (19) Konstantinidis, N. P. *Phys. Rev. B* **2007**, 76, 104434.
- (20) Bergomi, L.; Blaizot, J. P.; Jolicoeur, T.; Dagotto, E. *Phys. Rev. B* **1993**, 47, 5539–5542.
- (21) Joyes, P.; Tarento, R. J.; Bergomi, L. *Phys. Rev. B* **1993**, 48, 4855–4859.
- (22) Scalettar, R. T.; Moreo, A.; Dagotto, E.; Bergomi, L.; Jolicoeur, T.; Monien, H. *Phys. Rev. B* **1993**, 47, 12316–12319.
- (23) Willaime, F.; Falicov, L. M. *J. Chem. Phys.* **1993**, 98, 6369–6376.
- (24) Krivnov, V. Y.; Shamovsky, I. L.; Tornau, E. E.; Rosengren, A. *Phys. Rev. B* **1994**, 50, 12144–12151.
- (25) Sheng, D. N.; Weng, Z. Y.; Ting, C. S.; Dong, J. M. *Phys. Rev. B* **1994**, 49, 4279–4284.
- (26) Srinivasan, B.; Ramasesha, S.; Krishnamurthy, H. R. *Phys. Rev. B* **1996**, 54, 1692–1702.
- (27) Srinivasan, B.; Ramasesha, S.; Krishnamurthy, H. R. *J. Phys. Chem.* **1996**, 100, 11260–11269.
- (28) Ojeda, M. A.; Dorantes-Dávila, J.; Pastor, G. M. *Phys. Rev. B* **1999**, 60, 9122–9128.
- (29) Flocke, N.; Schmalz, T. G.; Klein, D. J. *J. Chem. Phys.* **2000**, 112, 8233–8240.
- (30) Lin, F.; Sørensen, E. S.; Kallin, C.; Berlinsky, A. J. *Phys. Rev. B* **2007**, 75, 075112.
- (31) Hubbard, J. *Proc. Roy. Soc. Lond. A* **1963**, 276, 238–257.
- (32) Pariser, R.; Parr, R. G. *J. Chem. Phys.* **1953**, 21, 767–776.
- (33) Pople, J. A. *Trans. Faraday Soc.* **1953**, 49, 1375–1385.
- (34) Schmalz, T. G. In *Valence Bond Theory*; Cooper, D. L., Ed.; Theoretical and Computational Chemistry; Elsevier: Amsterdam, 2002; Vol. 10; pp 535–564.

- (35) Hachmann, J.; Dorando, J. J.; Avilés, M.; Chan, G. K.-L. *J. Chem. Phys.* **2007**, *127*, 134309.
- (36) Gidofalvi, G.; Mazziotti, D. A. *J. Chem. Phys.* **2008**, *129*, 134108.
- (37) Rivero, P.; Jiménez-Hoyos, C. A.; Scuseria, G. E. *J. Phys. Chem. B* **2013**, *117*, 12750–12758.
- (38) Mizukami, W.; Kurashige, Y.; Yanai, T. *J. Chem. Theory Comput.* **2013**, *9*, 401–407.
- (39) Plasser, F.; Pašalić, H.; Gerzabek, M. H.; Libisch, F.; Reiter, R.; Burgdörfer, J.; Müller, T.; Shepard, R.; Lischka, H. *Angew. Chem. Int. Ed.* **2013**, *52*, 2581–2584.
- (40) Horn, S.; Plasser, F.; Müller, T.; Libisch, F.; Burgdörfer, J.; Lischka, H. *Theor. Chem. Acc.* **2014**, *133*, 1511.
- (41) Small, D. W.; Lawler, K. V.; Head-Gordon, M. *J. Chem. Theory Comput.* **2014**, *10*, 2027–2040.
- (42) Fukutome, H. *Int. J. Quantum Chem.* **1981**, *20*, 955–1065.
- (43) Löwdin, P.-O.; Mayer, I. *Adv. Quantum Chem.* **1992**, *24*, 79–114.
- (44) Hammes-Schiffer, S.; Andersen, H. C. *J. Chem. Phys.* **1993**, *99*, 1901–1913.
- (45) Stuber, J. L.; Paldus, J. In *Fundamental World of Quantum Chemistry. A Tribute Volume to the Memory of Per-Olov Löwdin*; Brandas, E. J., Kryachko, E. S., Eds.; Kluwer Academic Publishers: Dordrecht, The Netherlands, 2003; Vol. 1; pp 67–139.
- (46) Jiménez-Hoyos, C. A.; Henderson, T. M.; Scuseria, G. E. *J. Chem. Theory Comput.* **2011**, *7*, 2667–2674.
- (47) Yamaguchi, K.; Yamanaka, S.; Nishino, M.; Takano, Y.; Kitagawa, Y.; Nagao, H.; Yoshioka, Y. *Theor. Chem. Acc.* **1999**, *102*, 328–345.

- (48) Kawakami, T.; Takeda, R.; Nishihara, S.; Saito, T.; Shoji, M.; Yamada, S.; Yamanaka, S.; Kitagawa, Y.; Okumura, M.; Yamaguchi, K. *J. Phys. Chem. A* **2009**, *113*, 15281–15297.
- (49) Frisch, M. J.; Trucks, G. W.; Schlegel, H. B.; Scuseria, G. E.; Robb, M. A.; Cheeseman, J. R.; Scalmani, G.; Barone, V.; Mennucci, B.; Petersson, G. A. et al. Gaussian 09. Revision B.01, Gaussian Inc., Wallingford, CT, 2009.
- (50) Jiménez-Hoyos, C. A.; Rodríguez-Guzmán, R.; Scuseria, G. E. in preparation.
- (51) Jiménez-Hoyos, C. A.; Henderson, T. M.; Tsuchimochi, T.; Scuseria, G. E. *J. Chem. Phys.* **2012**, *136*, 164109.
- (52) Jiménez-Hoyos, C. A.; Rodríguez-Guzmán, R.; Scuseria, G. E. *J. Chem. Phys.* **2013**, *139*, 204102.
- (53) Tománek, D.; Frederick, N. C_n Fullerenes. <http://www.nanotube.msu.edu/fullerene/> (accessed Aug 1st, 2014).
- (54) Schwerdtfeger, P.; Wirz, L.; Avery, J. *J. Comput. Chem.* **2013**, *34*, 1508–1526.
- (55) Kokalj, A. *Comp. Mater. Sci.* **2003**, *28*, 155–168, code available from <http://www.xcrysden.org/>.
- (56) Löwdin, P.-O. *Phys. Rev.* **1955**, *97*, 1474–1489.
- (57) Mulliken, R. S. *J. Chem. Phys.* **1955**, *23*, 1833–1840.
- (58) Jensen, F. *Introduction to Computational Chemistry*; Wiley: New York, 1999.
- (59) Cárdenas, C.; Muñoz, F.; Muñoz, M.; Bernardin, A.; Fuentealba, P. *Phys. Chem. Chem. Phys.* **2012**, *14*, 14810–14814.
- (60) Raghavachari, K. *Chem. Phys. Lett.* **1992**, *190*, 397–400.
- (61) Piskoti, C.; Yarger, J.; Zettl, A. *Nature* **1998**, *393*, 771–774.

- (62) Jagadeesh, M. N.; Chandrasekhar, J. *Chem. Phys. Lett.* **1999**, *305*, 298–302.
- (63) Fowler, P.; Heine, T.; Rogers, K.; Sandall, J.; Seifert, G.; Zerbetto, F. *Chem. Phys. Lett.* **1999**, *300*, 369–378.
- (64) Fowler, P. W.; Mitchell, D.; Zerbetto, F. *J. Am. Chem. Soc.* **1999**, *121*, 3218–3219.
- (65) Ito, A.; Monobe, T.; Yoshii, T.; Tanaka, K. *Chem. Phys. Lett.* **2000**, *328*, 32–38.
- (66) Slanina, Z.; Uhlík, F.; Zhao, X.; Ōsawa, E. *J. Chem. Phys.* **2000**, *113*, 4933–4937.
- (67) Fan, M.-F.; Lin, Z.; Yang, S. *J. Mol. Struct.: THEOCHEM* **1995**, *337*, 231–240.
- (68) Lu, X.; Chen, Z. *Chem. Rev.* **2005**, *105*, 3643–3696.
- (69) Paulus, B. *Phys. Chem. Chem. Phys.* **2003**, *5*, 3364–3367.
- (70) Brabec, C. J.; Anderson, E. B.; Davidson, B. N.; Kajihara, S. A.; Zhang, Q.-M.; Bernholc, J.; Tománek, D. *Phys. Rev. B* **1992**, *46*, 7326–7328.
- (71) Feyereisen, M.; Gutowski, M.; Simons, J.; Almlöf, J. *J. Chem. Phys.* **1992**, *96*, 2926–2932.
- (72) Raghavachari, K.; Strout, D. L.; Odom, G. K.; Scuseria, G. E.; Pople, J. A.; Johnson, B. G.; Gill, P. M. W. *Chem. Phys. Lett.* **1993**, *214*, 357–361.
- (73) Grossman, J. C.; Mitas, L.; Raghavachari, K. *Phys. Rev. Lett.* **1995**, *75*, 3870–3873.
- (74) Taylor, P. R.; Bylaska, E.; Weare, J. H.; Kawai, R. *Chem. Phys. Lett.* **1995**, *235*, 558–563.
- (75) Bylaska, E. J.; Taylor, P. R.; Kawai, R.; Weare, J. H. *J. Phys. Chem.* **1996**, *100*, 6966–6972.
- (76) Wang, Z.; Day, P.; Pachter, R. *Chem. Phys. Lett.* **1996**, *248*, 121–126.
- (77) Martin, J. M. L.; El-Yazal, J.; François, J.-P. *Chem. Phys. Lett.* **1996**, *248*, 345–352.
- (78) Jones, R. O.; Seifert, G. *Phys. Rev. Lett.* **1997**, *79*, 443–446.

- (79) Murphy, R. B.; Friesner, R. A. *Chem. Phys. Lett.* **1998**, 288, 403–407.
- (80) Galli, G.; Gygi, F.; Golaz, J.-C. *Phys. Rev. B* **1998**, 57, 1860–1867.
- (81) Sokolova, S.; Lüchow, A.; Anderson, J. B. *Chem. Phys. Lett.* **2000**, 323, 229–233.
- (82) Prinzbach, H.; Weiler, A.; Landenberger, P.; Wahl, F.; Wörth, J.; Scott, L. T.; Gelmont, M.; Olevano, D.; v. Issendorff, B. *Nature* **2000**, 407, 60–63.
- (83) Saito, M.; Miyamoto, Y. *Phys. Rev. Lett.* **2001**, 87, 035503.
- (84) Lu, J.; Re, S.; Choe, Y.-k.; Nagase, S.; Zhou, Y.; Han, R.; Peng, L.; Zhang, X.; Zhao, X. *Phys. Rev. B* **2003**, 67, 125415.
- (85) Romero, A. H.; Sebastiani, D.; Ramírez, R.; Kiwi, M. *Chem. Phys. Lett.* **2002**, 366, 134–140.
- (86) Castro, A.; Marques, M. A. L.; Alonso, J. A.; Bertsch, G. F.; Yabana, K.; Rubio, A. *J. Chem. Phys.* **2002**, 116, 1930–1933.
- (87) Grimme, S.; Mück-Lichtenfeld, C. *Chem. Phys. Chem.* **2002**, 3, 207–209.
- (88) An, W.; Gao, Y.; Bulusu, S.; Zeng, X. C. *J. Chem. Phys.* **2005**, 122, 204109.
- (89) Zhang, C.; Sun, W.; Cao, Z. *J. Chem. Phys.* **2007**, 126, 144306.
- (90) Heaton-Burgess, T.; Yang, W. *J. Chem. Phys.* **2010**, 132, 234113.
- (91) Greene, K. R.; Beran, K. A. *J. Comput. Chem.* **2002**, 23, 938–942.
- (92) López-Sandoval, R.; Pastor, G. M. *Eur. Phys. J. D* **2006**, 38, 507–514.
- (93) Lin, F.; Sørensen, E. S.; Kallin, C.; Berlinsky, A. J. *Phys. Rev. B* **2007**, 76, 033414.
- (94) Lin, F.; Sørensen, E. S. *Phys. Rev. B* **2008**, 78, 085435.

- (95) Hedberg, K.; Hedberg, L.; Bethune, D. S.; Brown, C. A.; Dorn, H. C.; Johnson, R. D.; De Vries, M. *Science* **1991**, 254, 410–412.
- (96) Häser, M.; Almlöf, J.; Scuseria, G. E. *Chem. Phys. Lett.* **1991**, 181, 497–500.
- (97) Pulay, P.; Hamilton, T. P. *J. Chem. Phys.* **1988**, 88, 4926–4933.
- (98) Head-Gordon, M. *Chem. Phys. Lett.* **2003**, 372, 508–511.
- (99) Flocke, N.; Schmalz, T. G.; Klein, D. J. *J. Chem. Phys.* **1998**, 109, 873–880.
- (100) Bendikov, M.; Duong, H. M.; Starkey, K.; Houk, K. N.; Carter, E. A.; Wudl, F. *J. Am. Chem. Soc.* **2004**, 126, 7416–7417.
- (101) Lin, H. Q.; Campbell, D. K. *J. Appl. Phys.* **1991**, 69, 5947–5949.
- (102) Mikeska, H.-J.; Kolezhuk, A. K. In *Quantum Magnetism*; Schollwöck, U., Richter, J., Farnell, D. J., Bishop, R. F., Eds.; Lecture Notes in Physics; Springer: Berlin, 2004; Vol. 645; pp 1–83.
- (103) Essler, F. H. L.; Frahm, H.; Göhmann, F.; Klümper, A.; Korepin, V. E. *The One-Dimensional Hubbard Model*; Cambridge University Press: Cambridge, 2005.
- (104) Rodríguez-Guzmán, R.; Jiménez-Hoyos, C. A.; Schutski, R.; Scuseria, G. E. *Phys. Rev. B* **2013**, 87, 235129.
- (105) Mott, N. F. *Proc. Phys. Soc. A* **1949**, 62, 416.
- (106) Pastor, G. M.; Hirsch, R.; Mühlischlegel, B. *Phys. Rev. B* **1996**, 53, 10382–10396.
- (107) Scalmani, G.; Frisch, M. J. *J. Chem. Theory Comput.* **2012**, 8, 2193–2196.
- (108) Sheka, E. F.; Chernozatonskii, L. A. *J. Phys. Chem. C* **2007**, 111, 10771–10779.
- (109) Sheka, E. F.; Chernozatonskii, L. A. *Int. J. Quantum Chem.* **2010**, 110, 1466–1480.
- (110) Sheka, E. F.; Chernozatonskii, L. A. *Int. J. Quantum Chem.* **2010**, 110, 1938–1946.